IEEE Access
Multidisciplinary | Rapid Review | Open Access Journal

Received January 21, 2021, accepted February 25, 2021, date of publication March 8, 2021, date of current version March 17, 2021.

Digital Object Identifier 10.1109/ACCESS.2021.3064307

An Ultra-Miniaturized Antenna With Ultra-Wide Bandwidth Characteristics for Medical Implant Systems

MUHAMMAD YOUSAF[1], ISMAIL BEN MABROUK[2], (Senior Member, IEEE), MUHAMMAD ZADA[3], ADEEL AKRAM[1], YASAR AMIN[1], (Senior Member, IEEE), MOURAD NEDIL[4], (Senior Member, IEEE), AND HYOUNGSUK YOO[3,5], (Senior Member, IEEE)

[1]ACTSENA Research Group, Telecommunication Engineering Department, University of Engineering and Technology Taxila, Taxila 47050, Pakistan
[2]Department of Engineering, Durham University, Durham DH1 3LE, U.K.
[3]Department of Electronic Engineering, Hanyang University, Seoul 04763, South Korea
[4]Department of Electrical Engineering, University of Quebec in Abitibi-Témiscamingue, Val-d'Or, QC J9X 5E4, Canada
[5]Department of Biomedical Engineering, Hanyang University, Seoul 04763, South Korea

Corresponding author: Hyoungsuk Yoo (hsyoo@hanyang.ac.kr)

This work was supported in part by the Basic Science Research Program through the National Research Foundation of Korea funded by the Ministry of Education, Science and Technology under Grant 2019R1A2C2004774 and in part by the Abu Dhabi Department of Education and Knowledge (ADEK) Award for Research Excellence (AARE) 2018.

ABSTRACT In this study, an ultra–miniaturized implantable antenna based system with ultra-wideband characteristics in the industrial, scientific, and medical band (i.e., 2.4–2.48 GHz) is proposed for biomedical applications. A biocompatible and flexible liquid crystalline polymer material, Rogers ULTRALAM ($\tan\delta = 0.0025$ and $\varepsilon_r = 2.9$), is employed as both the substrate and superstrate. The proposed antenna with a compact size ($7 \times 7 \times 0.2$ mm^3) and a wide bandwidth (1533 MHz), was primarily designed for overcoming the detuning challenges that may occur owing to the electronic circuitry and irregularity as well as inhomogeneity of the human tissue environment. The miniaturization of this antenna was achieved by introducing a shorting pin and open-ended cuts in the ground plane, as well as in the radiating patch. The proposed antenna also yielded a higher gain and lower specific absorption rate (SAR). Through the link budget analysis, it was observed that 1 Mbps of data could be easily transmitted over a distance of 15 m. The simulated and in vitro measured results confirmed that compared to the recently reported antenna systems, our proposed ultra-wideband antenna based system could work more efficiently in the complex environment of the human body, thus establishing itself as an attractive candidate for biomedical applications.

INDEX TERMS Biocompatible, circuit, high gain, impedance, link budget, specific absorption rate, ultra-wideband.

I. INTRODUCTION

Implantable medical devices (IMDs) have attracted the attention of researchers because of the convenience they bring into a patient's life. IMDs may be intended for various medical applications such as glucose monitoring [1], retinal prosthesis [2], capsule endoscopy [3], and intracranial pressure monitoring [4]. These devices collect physiological data of the patient and establish wireless communication with an external controlling device through an implanted antenna. Compared to free-space antennas, implantable antennas have different radiation characteristics [5]. For example, the realized gain of implantable antennas is mostly below zero owing to the power loss in the surrounding tissues [6]. For IMDs, the robustness of the wireless link depends on the characteristics of the implanted antenna installed inside the IMDs [7]. Therefore, due consideration should be given to biocompatibility issues, safety concerns, compactness, and wider bandwidth in the design of an implanted antenna [8].

The MedRadio band with a frequency range of 401-406 MHz is often used for IMDs. However, owing to the bandwidth restrictions and limitations, this band is

The associate editor coordinating the review of this manuscript and approving it for publication was Nuno Garcia.

not suitable for the transmission of high-resolution images data. Additionally, IMDs operating in 433/868/915-MHz bands suffer a bulky size due to the larger wavelength, thus making them unsuitable for implantation in most scenarios. For example, the research interest in the area of wireless endoscopy (WE) has been increasing in recent years. Compared with the conventional (wired) endoscopy, the WE provides direct access to the whole small intestine and does not need any sedation [9]. However, a large-sized capsule could complicate the swallowing process and even threaten the patient's life. Therefore, the 2.4 GHz ISM band is mostly preferred for transmission of high-resolution images data from an IMD with a small-sized antenna [10]. It is likely that IMDs working in this band may face interference from nearby services, such as Wi-Fi, Bluetooth, IEEE 802.15.4, and near field communication. However, owing to the ultra-low powered transmitters of these short-range communication systems with different schemes of modulations and effective isotropic radiated power (EIRP), they have the very low ability of influencing other wireless equipment or IMDs [11].

Recently, various techniques such as periodic structures [12], split ring resonator [13], and lengthening the current path [14] were developed by various researchers for the miniaturization of an implantable antenna. In this study, the volume of the proposed ultra-wideband antenna was confined to 9.8 mm^3 by introducing open-ended cuts in the patch, and also in the ground plane. A shorting-pin, which acts similar to a ground plane by doubling the size of the antenna [15] was also used. Similarly, owing to the IMDs circuitry, as well as the heterogeneity of human tissues, the antenna integrated with an IMD may detune from its operating band [16]. Furthermore, with aging, the properties of the human body vary, and can also cause detuning of the antenna. Therefore, wideband antennas with stable radiation characteristics are always recommended for IMDs. Several recent studies have suggested different methods for designing wideband antennas for biomedical applications [17]–[19]. The authors in [17] have achieved a total bandwidth of 120 MHz in the MedRadio band by employing meandered strips. Likewise, in [18], a sigma-shaped radiator was coupled with a C-shaped ground to obtain a wider bandwidth of 337 MHz in the MedRadio band. In [20], the authors designed a circularly polarized wideband antenna operating in the 0.915 GHz ISM band for endoscopic applications. Circular polarization (CP) was achieved by creating a helical structure and by placing the proposed antenna in the wrapped form with the inner wall of the capsule. However, despite its bulky volume (66.7 mm^3) and complex geometry, the suggested CP antenna exhibits a lower gain of −19.6 dBi and narrow bandwidth of 185 MHz. Moreover, this wrapped conformal antenna can pose difficulties in integration with internal circuitry. In fact, the signal propagation in a human body is better at lower frequencies; however, the radiated power allowed in the lower bands is smaller than the higher frequency bands [15], thus, imposing power constraints.

A multiple input multiple output (MIMO) implantable antenna operating at 2.45 GHz and having a peak gain of −15.18 dBi was proposed in [21]. Although, the achieved gain was satisfactory, the suggested antenna was excited with four ports, which could increase its complexity and incompatibility with the modern IMDs. A wideband circular-shaped antenna resonating at 2.4 GHz with a bandwidth of 330 MHz was designed in a seven-layered brain phantom [22]. However, its specific absorption rate (SAR) was high enough to threaten the patient's safety during a relatively long checkup. Furthermore, despite having a larger volume (39.3 mm^3), the reported antenna had a low peak gain of −20.75 dBi. A wideband dipole antenna operating at 915 MHz was examined recently for tongue-controlled systems [16]. The impedance matching was achieved primarily by embedding a 11 pF capacitor at the rear side of the antenna. However, the geometrical structure of the antenna was not suitable for its integration with most of the IMDs; in addition, the usage of the capacitor has complicated the suggested design. Furthermore, a thin layer (0.1 mm) of PDMS was used to coat the antenna, which could not be maintained for a long-term usability in IMDs unlike the tongue drive system (semi-implantable device).

In this work, we present an ultra-miniaturized implantable antenna system with ultra-wide bandwidth characteristics in the industrial, scientific, and medical (ISM) band of 2450 MHz. The proposed miniaturized antenna has a compact volume of 9.8 mm^3, which is achieved by inserting a shorting pin and etching open-ended cuts in the radiator, as well as in the ground plane. Two resonance modes were combined to attain a wide bandwidth of 1533 MHz, which renders it immune to the detuning effects that may occur due to environmental heterogeneity and IMD circuitry. The combination of the two resonance modes was made possible through step wise modifications in the design. The initial design and analysis of our suggested ultra-wideband antenna were carried out in the center of a homogeneous skin phantom (HSP) with the dimensions of 25 mm × 25 mm × 25 mm. Subsequently, the HSP results were validated through further simulations in different heterogeneous parts, such as the head, arm, and leg of a human body with a finite difference time domain (FDTD) based simulator. For ensuring the patient safety, the SAR was investigated in the FDTD based simulator and was found to be compliant with IEEE safety guidelines for various implanted organs. For monitoring the biological signals, the reliability of the wireless link was validated through the link budget calculations for three implant locations. Table 1 shows the novelty of our ultra-miniaturized and ultra-wideband antenna by comparing its performance parameters with those of the other implantable antennas that have been reported recently in literature. It is evident that in spite of its simple shape, the proposed antenna exhibits prominent features with considerably less volume and ultra-wide bandwidth characteristics as compared to other antennas. The reflection coefficients (S_{11}) obtained in different simulation scenarios were

TABLE 1. Comparison of the proposed ultra-wideband implantable antenna with previous studies.

Ref.	Year	Frequency (GHz)	Volume (mm^3)	Bandwidth (MHz)	Gain (dBi)	SAR (W/kg)		Phantom size (mm)	Implantation depth (mm)	Operating condition
						1-g	10-g			
[2]	2004	2.45	18	3	-27.4	1.158	--	--	--	Heterogeneous
[19]	2018	2.45	40	1395	-9	131	--	80 × 80 × 80	40	Heterogeneous
[21]	2018	2.45	434.6	440	-15.18	--	--	80 × 80 × 51.2	19.5	Heterogeneous
[22]	2019	2.4	39.3	330	-20.75	568.2	84.2	100 × 100 × 72.2	10	Heterogeneous
[23]	2015	2.45	127	190	--	--	--	90 × 90 × 25	4	Homogeneous
[24]	2019	2.45	99.75	520	-26.4	712.1	--	80 × 80 × 25	4	Homogeneous
[25]	2015	2.45	292.7	--	-18.4	0.29	--	--	--	Homogeneous
[26]	2019	2.60	36.96	400	-19.7	0.719	--	--	4	Homogeneous
[27]	2019	2.45	295.7	200	-23	38.2	--	100 × 100 × 100	10	Heterogeneous
[35]	2021	2.45	2.11	152.8	-24.5	233.2	27.7	100 × 100 × 100	50	Homogeneous
[36]	2020	2.45	10.668	877.1	-9.81	524.3	50.2	100 × 100 × 100	4	Homogeneous
[37]	2019	2.45	17.15	219	-18.2	305	81.7	100 × 100 × 100	3	Homogeneous
This work	2020	2.45	9.8	1533	-15.8	350.81 (Leg)	--	25 × 25 × 25	12.5	Homogeneous/ Heterogeneous

validated by testing a fabricated prototype of the antenna and its corresponding system in a saline solution. For the measurements of the radiation patterns, the same prototypes were placed in a container containing minced pork to mimic the human body tissues. Tests on the prototyped antenna and its system confirmed a close agreement between the simulated and measured results.

II. METHODOLOGY

A. THEORETICAL BACKGROUND

As a medium, a human body possesses various challenges for wireless transmission. It is made of different tissues (skin, fat, muscle, and bone) with variable permittivity and electrical conductivity that are unpredictable and change with the loss or gain of weight, patient age, or even with changing postures [28]. Furthermore, the location of the IMDs is also varying. During surgery, the IMD is kept at the most suitable location to perform its basic functions. Owing to all these factors, the antenna implanted in the human body may detune from its operating frequencies. Therefore, in this research, an ultra-wideband implantable antenna having stable radiation characteristics, irrespective of the implantation scenario is proposed for IMDs. Initially, the design of the proposed implantable antenna for the operation at 2.45 GHz was estimated by the formula given below [19].

$$f_r = \frac{c}{\lambda_g \sqrt{\varepsilon_{eff}}} \approx \frac{c}{L_g \sqrt{\frac{\varepsilon_r + 1}{2}}} \tag{1}$$

where f_r, c, λ_g, and ε_{eff} represent the resonance frequency, speed of the EM waves in free-space, guided wavelength or wavelength in a medium other than free-space, and effective permittivity, respectively. Similarly, L_g denotes the length of the antenna and ε_r is the combined relative dielectric constant of the superstrate and substrate. Then, miniaturization techniques were adopted for reducing the size of the designed antenna to make it suitable for employment in modern miniaturized IMDs. A shorting-pin doubles the size of the antenna, and hence, aids in its miniaturization. Similarly, the capacitance gets increased due to slots insertion in the ground plane, thus providing a further possibility of miniaturization [15]. Therefore, a shorting-pin with a 0.3 mm radius and a slotted-ground plane were employed in the reported design. The superstrate in our design was primarily employed for decoupling the antenna from the lossy surroundings by avoiding a direct contact of its radiator with the human tissue [7], [19]; however, it also assisted in the miniaturization as observed by the authors in [29].

TABLE 2. Dielectric properties of different parts of human body at 2.45 GHz.

Tissue type	Permittivity (ϵ_r)	Conductivity [σ (S/m)]
Bone	11.4	0.394
Muscle	52.7	1.74
Fat	10.8	0.268
Skin	38	1.46

The dielectric constant (ε_r) and conductivity (σ) of different components of a human body at 2.45 GHz are tabulated in Table 2. The high ε_r of the human tissues influences the effective dielectric constant [19]. The ε_r also affects the wavelength (λ) of an electromagnetic wave, thereby helping in miniaturization. In the free-space, λ can be calculated as

$$\lambda = \frac{c}{f_r} \tag{2}$$

However, in a medium other than free-space, λ is reduced due to high permittivity values as obvious from the following

equation [28].

$$\lambda_g = \frac{\lambda}{\sqrt{\varepsilon_r}} \tag{3}$$

For instance, at 2.45 GHz, λ in free-space is 122.44 mm; however, it is only 19.9 mm in the skin with $\varepsilon_r = 38$. This is significantly worthful in designing implantable antennas where miniaturization is a crucial aspect. Consequently, the overall volume of the designed antenna was reduced to 9.8 mm^3, making it the smallest antenna that offered a stable impedance matching with ultra-wide bandwidth characteristics. Furthermore, the σ of the body parts is more than the air. Its impact is similar to immersing the IMD in seawater, i.e., the signal will be attenuated while passing through the body parts [30]. This leads to a shorter communication range owing to the reduction in penetration depth [28].

B. LAYOUT OF THE PROPOSED ULTRA-WIDEBAND ANTENNA AND CORRESPONDING SYSTEM

The front and rear configuration of our proposed ultra-wideband antenna are portrayed in Figs. 1(a) and (b), respectively. To attain the targeted frequency and ultra-wide bandwidth, several cuts were etched from a square-shaped radiating patch to give it a meander line structure, and thus lengthen the current flow path, which assists in miniaturization. To provide biocompatibility, Rogers ULTRALAM 3850HT (tan$\delta = 0.0025$, $\varepsilon_r = 2.9$, and thickness $= 0.1$ mm) of size 7×7 mm^2 was chosen for the substrate and superstrate of the suggested antenna. The antenna was excited from the patch center through a 50 Ω feed with a 0.3 mm radius.

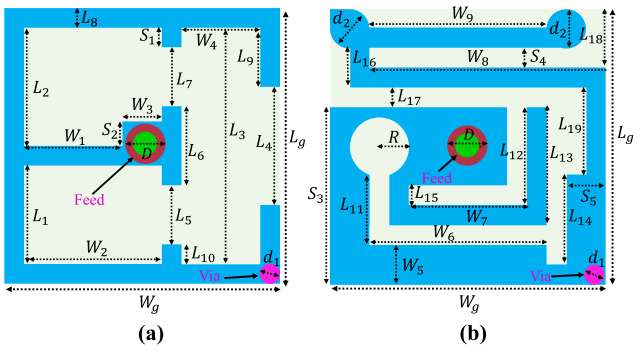

FIGURE 1. Geometry of the ultra-wideband antenna. (a) Patch. (b) Ground.

Table 3 provides all the optimized design parameters of the proposed antenna. It was observed in the simulations that the side strip width (W_5) in the ground plane and the parameters (L_1 and L_4) of the resonator were crucial for tuning and impedance matching of the designed ultra-wideband implantable antenna. Therefore, these parameters were specifically optimized for achieving the desired bandwidth. Similarly, we also observed that other variables, such as L_3, S_1, and R have minimal effects; however, they can be used as accessorial parameters with L_1, L_4, and W_5 in tuning and impedance matching. It is noteworthy that the

TABLE 3. Parameters of the proposed antenna (units: *mm*).

Parameters	Values	Parameters	Values	Parameters	Values
L_g	7.0	L_{13}	3.0	W_6	4.5
L_1	2.5	L_{14}	2.0	W_7	3.0
L_2	3.0	L_{15}	0.5	W_8	6.0
L_3	6.0	L_{16}	1.0	W_9	4.5
L_4	3.0	L_{17}	0.5	S_1	0.5
L_5	1.37	L_{18}	1.5	S_2	0.62
L_6	2.0	L_{19}	2.5	S_3	4.5
L_7	1.5	W_g	7.0	S_4	0.5
L_8	0.5	W_1	2.5	S_5	1.0
L_9	1.5	W_2	3.5	d_1	0.3
L_{10}	0.63	W_3	1.0	d_2	0.5
L_{11}	1.8	W_4	2.0	R	0.75
L_{12}	2.5	W_5	1.0	D	1.0

dimensions of all the design parameters for the patch and the ground plane were selected satisfactorily after conducting a detailed parametric study on the basis of stable S_{11}.

In real scenarios, the IMDs not only hold the antenna but also other electronic components, for example, circuitry, power sources, electronics pack, and sensors. Hence, the designed ultra-wideband antenna was installed in a skin implantable system, as displayed in Fig. 2. The designed system contains microelectronic components, upper and lower lids, two batteries, and housing within a volume of 14 mm × 8 mm × 5 mm (560 mm^3). A perfect electric conductor (PEC) material is considered for the batteries and electronics components, while the circuit PCB was fabricated on Roger RT/duriod 6010. All the components (including the ultra-wideband antenna) were encapsulated in ceramic alumina (Al_2O_3). Al_2O_3 ($\varepsilon_r = 9.8$ and thickness $= 0.25$ mm) is a suitable material for biomedical applications due to its biocompatible nature.

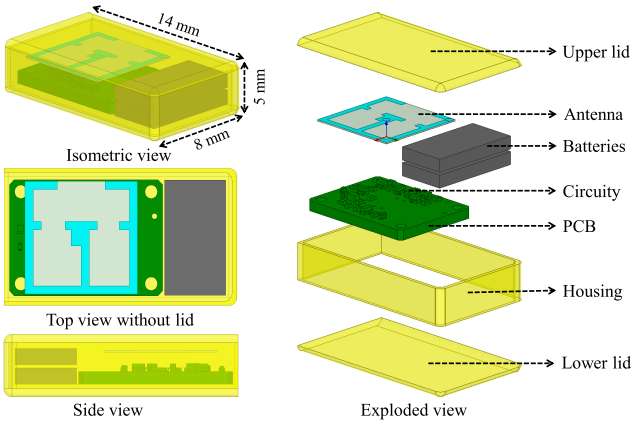

FIGURE 2. The architecture of the ultra-wideband antenna based system.

C. DESIGNING STEPS

The proposed ultra-wideband antenna was optimized and evolved in four steps as described in Fig. 3. The corresponding S_{11} comparison for the steps involved is illustrated in Fig. 4. As obvious from the successive steps, the proposed

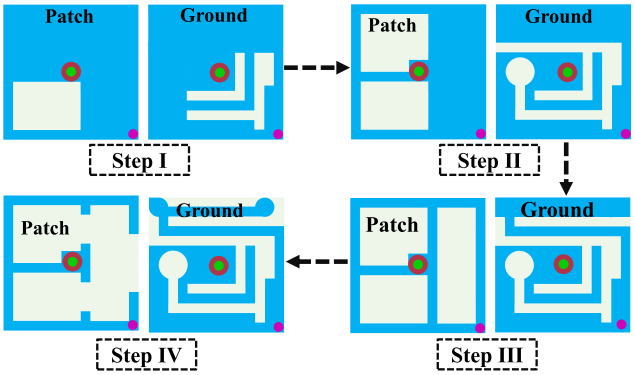

FIGURE 3. Steps in the design of the ultra-wideband antenna.

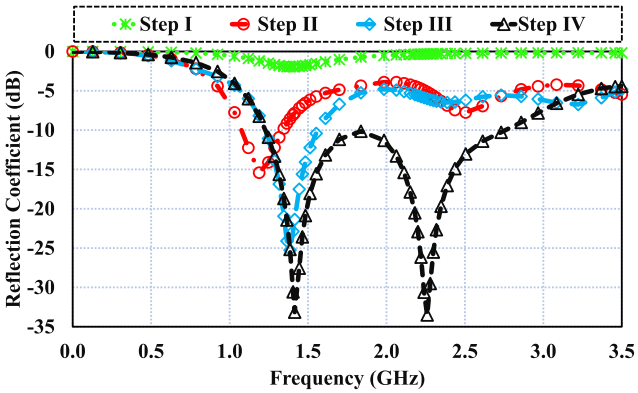

FIGURE 4. Comparison of S_{11} for the four steps to achieve a wide bandwidth.

designed was initiated from a simple patch antenna with slots in the radiator and the ground plane. It was observed that a weak resonance with $S_{11} > -3.5$ dB appeared at 1.65 GHz in step I due to insertion of the via and the slots in the metallic parts of the antenna. As mentioned earlier, the capacitance increases due to the slots in the patch or ground, thus shifting the resonance frequency to the lower values. Therefore, the resonance mode that appeared in step I was moved to 1.2 GHz in step II by etching further slots in the ground plane and the patch. Furthermore, a second resonance was generated at approximately 2.4 GHz. By inserting an open-ended slot in the ground and a rectangular cut in the patch in step III, the second resonance that appeared in step II at approximately 2.4 GHz was shifted to 2.36 GHz. Finally, through modifications in step IV, the upper resonance appearing at approximately 2.4 GHz in the S_{11} plot corresponding to step II, was successfully combined with the lower fundamental resonance mode. Thus an ultra-wide bandwidth of 1533 MHz was achieved. Furthermore, it can be observed from Fig. 4 that the step-wise modifications improved the impedance matching of the designed antenna.

D. EQUIVALENT CIRCUIT MODEL

To comprehend the wideband characteristics of the ultra-wideband antenna, an equivalent circuit model was

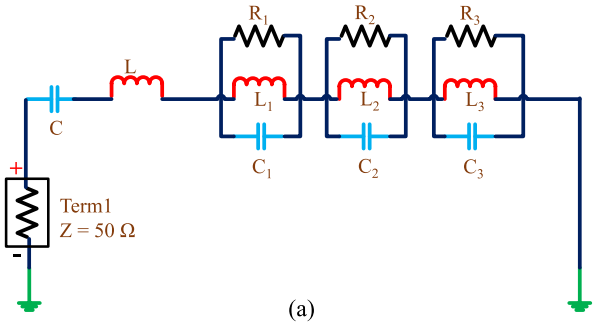

Parameters symbols and values (Units = Ω, nH, pF)

C	L	R_1	L_1	C_1	R_2	L_2	C_2	R_3	L_3	C_3
1.245	4.89	32	2.574	4	57	2.32	3.1	83.8	1.316	0.754

(b)

FIGURE 5. (a) Equivalent circuit of the ultra-wideband antenna. (b) Corresponding values of the electrical components employed in the circuit.

developed in the advanced design system (ADS) software as displayed in Fig. 5(a). This circuit is based on the degenerated Foster canonical (DFC) model, which is widely applicable for ultra-wideband antennas characterization. An antenna with wideband characteristics can be considered as a radiating element producing several closely associated resonances, in which some adjacent bands overlap with each other [16]. Each resonance band can be analyzed using RLC lumped elements connected in parallel. To obtain a wideband feature, multiple parallel-connected RLC circuits, with closely associated bands can be joined in series. In Fig. 5(a), C and L represent the capacitance and inductance, respectively, when the ultra-wideband antenna is resonating at the fundamental lower mode. The three parallel RLC circuits connected in series realize the remaining upper resonances. The three resistors R_1, R_2, and R_3 correspond to the radiation resistances of the related resonances. The left RLC circuit, comprising R_1, C_1, and L_1 controls the impedance matching within the operating band; the middle RLC tank comprising R_2, C_2, and L_2 adjusts the lower side of the ultra-wideband; and the right RLC circuit comprising R_3, C_3, and L_3 controls the upper frequencies. The values of the electrical components employed in the equivalent circuit are given in the table shown in Fig. 5(b).

E. SIMULATION AND TESTING SETUPS

Initially, the suggested ultra-wideband antenna system was designed and evaluated in HFSS software in a homogeneous skin phantom (HSP) as visualized in Fig. 6(a). The antenna was kept in the center of the HSP and the distance between the antenna and the air, in this case, was about 12.5 mm. The ε_r and σ values assigned to the HSP at 2.45 GHz band were 38 and 1.46 S/m, respectively. To consider a more realistic and practical scenario, the ultra-wideband antenna system was implanted in the arm, head, and leg of a heterogeneous

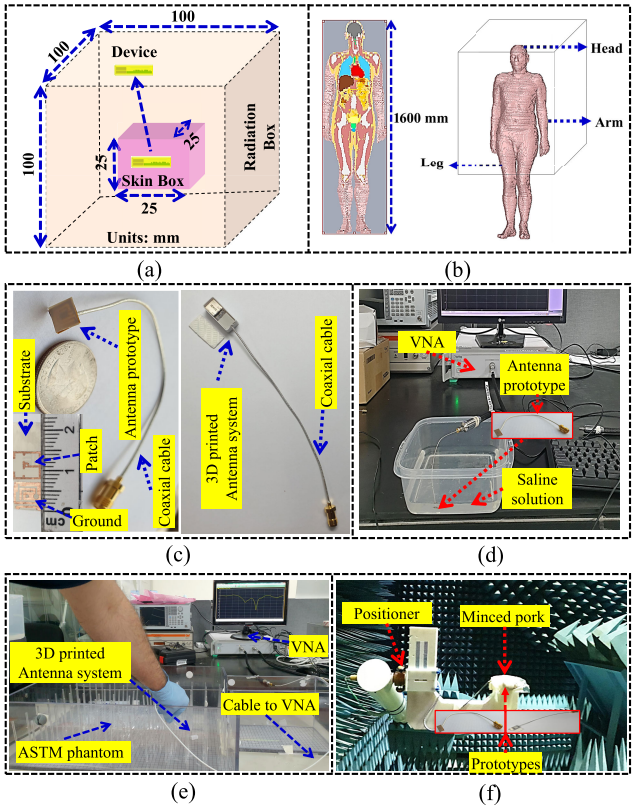

FIGURE 6. Simulation and test setups (units: mm): (a) Homogeneous skin phantom. (b) Realistic hetrogeneous human models. (c) Fabricated prototypes. (d) S_{11} measurement setup for the antenna. (e) S_{11} measurement setup for the system. (f) Radiation patterns measurement setup for the antenna and corresponding system.

model as shown in Fig. 6(b). The performance of the reported antenna was evaluated in terms of S_{11}, radiation patterns, SAR, and communication link margins in the aforementioned scenarios. For validating the results obtained from the simulation scenarios, the prototypes of the ultra-wideband antenna and system were fabricated and are depicted in Fig. 6(c). The S_{11} of the antenna was measured in a container filled with saline solution through the vector network analyzer as shown in Fig. 6(d), while that of the entire 3D system was measured in the American Society for Testing Materials (ASTM) phantom filled with saline solution, as shown in Fig. 6(e). Furthermore, as visualized in Fig. 6(f), the radiation pattern measurements of the antenna with and without the corresponding system was conducted at 2.45 GHz in minced pork to mimic the human tissue properties approximately.

F. SENSITIVITY ANALYSIS OF THE PROPOSED ULTRA-WIDEBAND ANTENNA

As already discussed, an implantable antenna is surrounded by human tissues; therefore, its performance is dependent on their properties. As a result, the performance of the antenna under different tissue loading conditions must be examined for accurate evaluation. For this purpose, the ε_r and σ of the

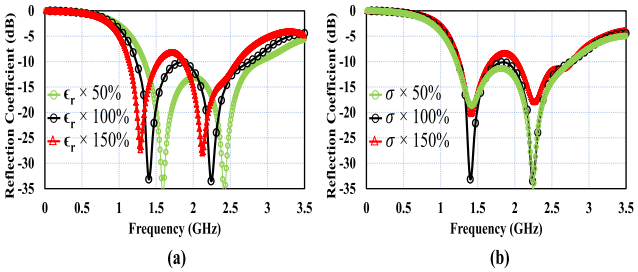

FIGURE 7. Sensitivity analysis as a function of, (a) ε_r. (b) σ.

HSP are varied from 50% to 150%, as shown in Figs. 7(a) and (b), respectively.

The S_{11} curves in Fig. 7(a) show that the achieved bandwidth moves to the left side as ε_r increases, while a shift towards the higher frequencies is observed for a decrement in ε_r. This phenomenon is well consistent with the inverse relationship between ε_r and f_r in Eq. (1). Meanwhile, it is investigated that σ has minimal effects on the working frequencies, as shown in Fig. 7(b). According to Eq. (1), the σ could not directly influence the operating frequencies, as shown in Fig. 7(b). However, the variations in σ as well as in ε_r of the tissues affect the impedance matching of the antenna [31], thereby increasing/decreasing the S_{11} depth (Figs. 7(a) and (b). Furthermore, σ and ε_r also affect the tanδ of the tissues. The relationship between tanδ, σ, and ε_r can be given by [31].

$$tan\delta = \frac{\sigma}{\varepsilon_r \varepsilon_o \omega} \tag{4}$$

where ε_o and ω represent the free-space permittivity and radian frequency, respectively.

G. PARAMETRIC ANALYSIS

Parametric analysis of the antenna is crucial for its optimization, as well as for selecting the optimum dimensions of its parameters based on the scenario. This parametric analysis was carried out in the same HSP as visualized in Fig. 6(a). The ultra-wideband antenna was kept at the center of the HSP to examine the effects of the variations in its parameters on S_{11}. For the proposed ultra-miniaturized antenna, the important design parameters for the parametric study are the shorting-pin position, the lengths (L_1 and L_4) of the patch slots, and the width (W_5) of the ground strip as portrayed in Figs. 1(a) and (b). It is noteworthy that apart from these mentioned parameters, all the other dimensional parameters for the radiator and the ground plane were also selected satisfactorily on the basis of a detailed parametric study in terms of S_{11}.

1) EFFECT OF VARYING THE SHORTING-PIN POSITION

The effect of the variation in the shorting-pin position on the S_{11} and impedance matching are visualized in Figs. 8(a) and (b), respectively. It can be clearly seen that the shorting-pin position affected the impedance matching

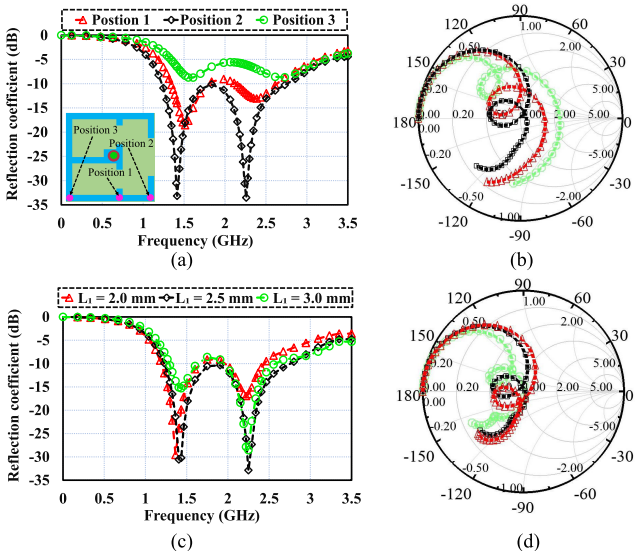

FIGURE 8. Influence of variations in shorting-pin position on (a) S_{11} and (b) impedance matching. Influence of variations in L_1 on (c) S_{11} and (d) impedance matching.

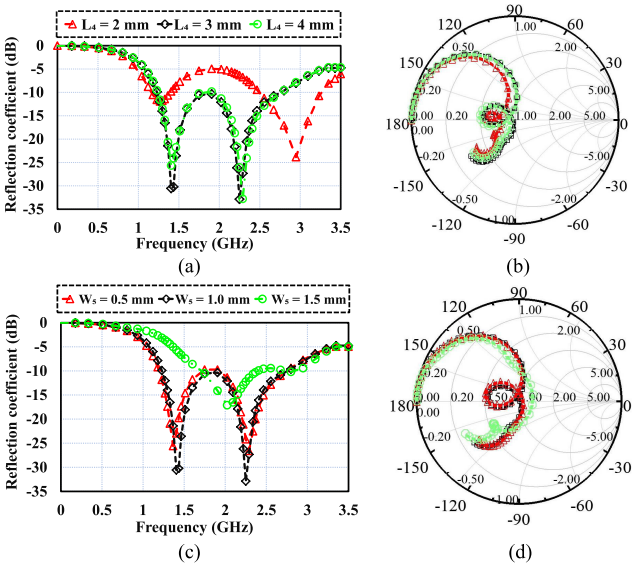

FIGURE 9. Influence of variations in L_4 on (a) S_{11} and (b) impedance matching. Influence of variations in W_5 on (c) S_{11} and (d) impedance matching.

of the antenna in the wide operating bandwidth that was achieved. The matching of the proposed ultra-wide antenna disturbed as the shorting pin moved from the right corner towards the left corner. To better understand this, the impedances of these shorting pin positions are drawn in the smith chart (Fig. 8(b)). At position 3, the antenna has an inductive impedance, thus it is necessary to move down the loop of the impedance loci in order to decrease the inductance. Therefore, the shorting pin was moved from the right corner towards the left corner. The impedance loci created a pigtail shape loop in the middle of the smith chart, which is responsible for achieving the wide bandwidth characteristics. This analysis suggested that the lower right corner is the optimal choice to encompass the targeted ultra-wideband.

2) EFFECT OF VARYING THE LENGTH L_1 OF THE PATCH SLOT

L_1 of the patch slot was varied from 2–3 mm. Fig. 8(c) exhibits the ultra-wideband antenna behavior in terms of the S_{11} as a function of L_1. It is obvious that the operating ultra-wideband of the antenna shifted to the right side of the frequency spectrum when L_1 was increased from 2 to 3 mm. We further observed that apart from tuning the frequencies, L_1 can also be utilized for impedance matching of the proposed antenna, as shown by using the smith chart in Fig. 8(d). A slight move up tendency in the loop of the impedance loci was observed from capacitive to inductive impedance when L_1 was increased from 2 to 3 mm. However, the size of the impedance loop increased at $L_1 = 2.5$ mm, which implies a wide and stable impedance matching in the considerable frequency range.

3) EFFECT OF VARYING THE LENGTH L_4 OF THE PATCH SLOT

L_4 had a prominent influence on S_{11} because it stabilized the impedance matching and current flow of the antenna. L_4 was varied from 2–4 mm to achieve the desired wideband characteristics. Fig. 9(a) depicts the influence of L_4 on S_{11}. It can be observed that a lower value of L_4 (i.e., 2 mm) strongly degraded S_{11} of the antenna. This effect was more prominent at lower frequencies than at higher frequencies. However, by increasing L_4, the frequency bands were shifted to the desired frequencies and provided a stable impedance matching in the entire frequency range of interest. Furthermore, it was observed that for $L_4 > 3$ mm, the depth of the lower resonance decreased significantly. The influence of L_4 on impedance matching is shown in Fig. 9(b) using the smith chart. As can be seen that the impedance loop is not much sensitive to $L_4 > 3$ mm values. However, the impedance loop shrank at $L_4 = 2$ mm due to stronger coupling between strips. Hence, we kept the value of L_4 as 3 mm.

4) EFFECT OF VARYING THE WIDTH W_5 OF THE GROUND SIDE STRIP

Although the antenna performance was very sensitive to the patch slots, the ground slots can also play a significant role in achieving wideband characteristics in the desired frequency band. Therefore, the parameter W_5 was varied from 0.5–1.5 mm and observed that it had a greater influence on S_{11} and impedance matching compared to the other ground slot parameters. Fig. 9(c) shows the effects of changing the side strip width W_5 on S_{11}. It can be observed that when W_5 was increased to 1.5 mm, the gap between the nearby strips would decrease which in turn, would enhance the coupling. As a result, the antenna performance would degrade as a consequence of lowering the impedance depth. This effect can be seen in Fig. 9(d) from the smith chart. The small gap between nearby strips increased the capacitance as the impedance loop shifted away from the center of the

smith chart towards the capacitive region and the frequency shifted to the higher spectrum. However, by keeping W_5 at 0.5 mm, provided enough gap to decouple the nearby strip lines. Therefore, it resulted in stable and broad bandwidth characteristics for the proposed antenna at the corresponding ISM band of 2.45 GHz.

III. RESULTS AND DISCUSSION

The focus of this work was to design a miniaturized antenna system with ultra-wide bandwidth having impedance stability and operating at 2.45 GHz, which would mitigate the detuning challenges by perfectly working inside the human body. The antenna system was simulated and measured using the setups displayed in Fig. 6 in FEM– and FDTD–based simulators. The parameter S_{11} of the ultra-wideband antenna, which was simulated and measured in different scenarios is depicted in Fig. 10. It is obvious that the reported antenna maintained the impedance matching stability over a wideband for all the simulated and measured scenarios. The achieved bandwidths in the simulation were 1567, 1591, 1557, and 1533 MHz for the head, arm, leg, and HSP, respectively. S_{11} was measured in a container filled with saline solution and the bandwidth obtained in the measurement was in good agreement with those obtained from various simulated scenarios. The bandwidth attained in the measurement was 1770 MHz. Similarly, Fig. 11 shows the S_{11} comparison of the ultra-wideband antenna based system in various environments. From these investigations, it can be concluded that the proposed ultra-wideband antenna can indeed, be a good candidate for utilization in IMDs.

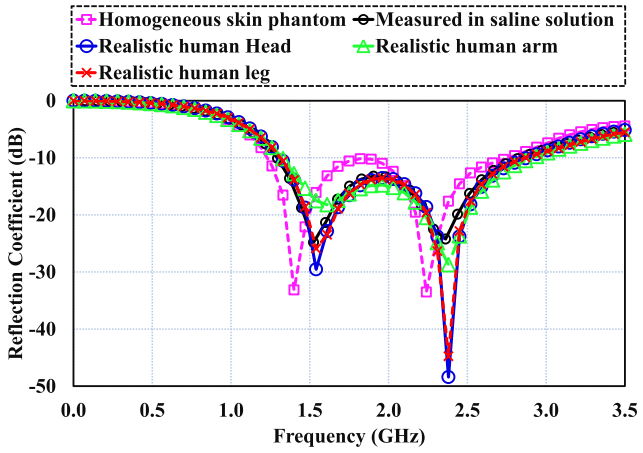

FIGURE 10. Comparison of S_{11} of the antenna in different scenarios.

The radiation patterns of the ultra-wideband antenna obtained through simulations in different scenarios and measurement in minced pork are visualized in Fig. 12. It can be seen that regardless of the simulation and measured environment, the gain polar patterns were almost same; however, the maximum values are depended on the implantation sites. The radiation patterns achieved at 2.45 GHz were approximately omni-directional in both the H- and E-planes for all

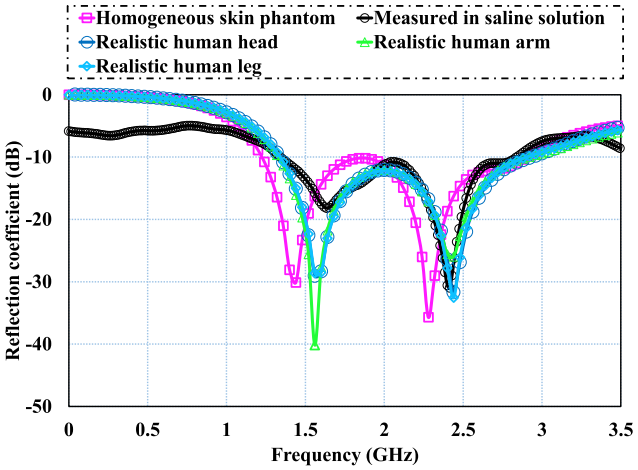

FIGURE 11. Comparison of S_{11} of the antenna system in different scenarios.

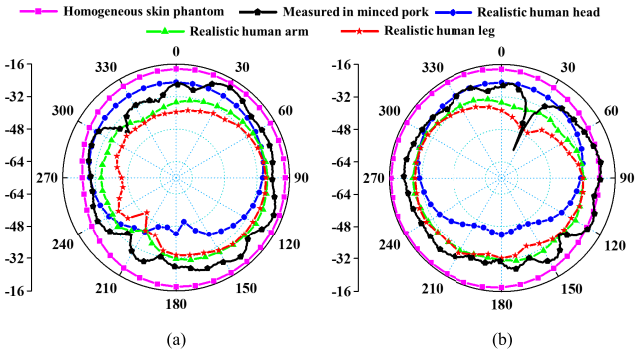

FIGURE 12. Comparison of polar patterns of the antenna in different scenarios at 2.45 GHz. (a) E-plane. (b) H-plane.

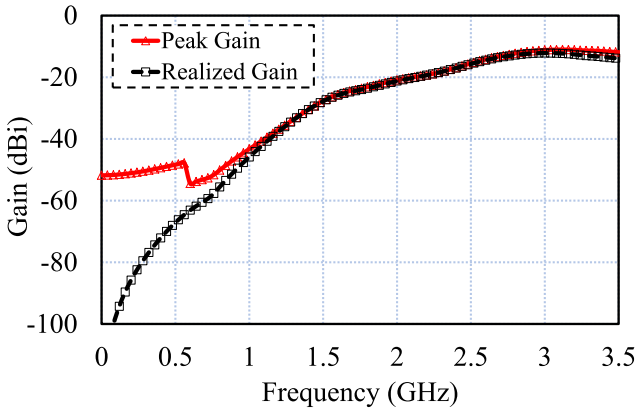

FIGURE 13. Comparison of the peak and realized gains.

the scenarios. In minced pork, the peak gain was observed to be −20.3, whereas in the simulations, it was −15.8, −25, −26.3, and −27.8 dBi in the HSP, head, arm, and leg, respectively. Fig. 13 shows the comparison of the peak and realized gains. From Fig. 13, it can be clearly seen that the gain of the proposed ultra-wideband antenna maintains a broadband performance. However, a slight difference between peak and

TABLE 4. Performance summary of the proposed antenna and its corresponding system in ISM band (2.45 GHz).

Parameter	HSP		Head		Arm		Leg		Measured	
	Antenna	System	Antenna	System	Antenna	System	Antenna	System	Antenna	System
BW (MHz)	1533	1680	1567	1600	1591	1560	1557	1610	1770	1525
Gain (dBi)	-15.8	-16	-25	-26.6	-26.3	-28.4	-27.8	-25.4	-20.3	-22

realized gain was observed, which is due to the material and feeding losses [32]. Furthermore, the radiation patterns of the entire system were also simulated and measured in the same scenarios used for the antenna without the system. For the conciseness of this manuscript, the radiation patterns with system are not displayed. However, the performance of the antenna and its corresponding entire system is summarized in Table 4, in terms of its bandwidth and gain in different scenarios. The difference between the achieved gain values may be attributed to the different implantation depths and phantom sizes in the given scenarios. It is noteworthy that the consequences of different environments on the results of the ultra-wideband antenna and the corresponding system were minimal. This further emphasizes its use in IMDs.

To ensure the safety of patients wearing IMDs, the ICNRP and IEEE C95.1-1999 limit the peak average SAR for 1 and 10 g of tissues to 2 and 1.6 W/kg, respectively [33]. To comply with IEEE safety guidelines, we carried out SAR analyses at three different locations (i.e., head, arm, and leg) in the human body model. For these analyses, the input power to the proposed implantable antenna was set at 1 W. The calculated SAR and maximum allowable input power values at the ISM band of 2.45 GHz in the aforementioned implant locations are listed in Table 5. Additionally, the SAR distributions at the prescribed locations are plotted in Fig. 14(a)–(c). A maximum SAR of 350.81 W/kg with a maximum allowable power of 4.56 mW was observed in the leg tissues. The increase in SAR in the leg tissue was expected owing to its highly conductive nature. Nevertheless, the calculated SAR values of the proposed antenna meet the safety guidelines, and hence, it is not an issue to be focused on in this study.

TABLE 5. 1-g peak SAR and maximum allowable power in ISM (2.45 GHz) band.

Body tissue	Peak SAR(W/kg)	Max. allowable input power (mW)
Head	289.76	5.52
Leg	350.81	4.56
Arm	282.63	5.66

A. COUPLING ANALYSIS

Owing to the presence of the device circuitry in the closeness of the antenna, it is mandatory to investigate the coupling issues between the device components and the recommended ultra-wideband antenna. To analyze the effects and to determine the minimum gap between the device components and antenna, the distance (D) between the electronics circuitry and ultra-wideband antenna is varied, as demonstrated by Fig. 15. When D decreases, the performance of the ultra-wideband antenna degrades. Therefore, the proposed ultra-wideband antenna should be placed at least 0.6 mm away from the metallic components of the system for avoiding performance deterioration.

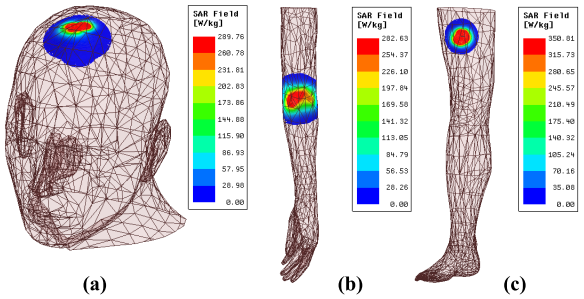

FIGURE 14. Average SAR distributions over 1 g of tissue at 2.45 GHz. (a) Head. (b) Arm. (c) Leg.

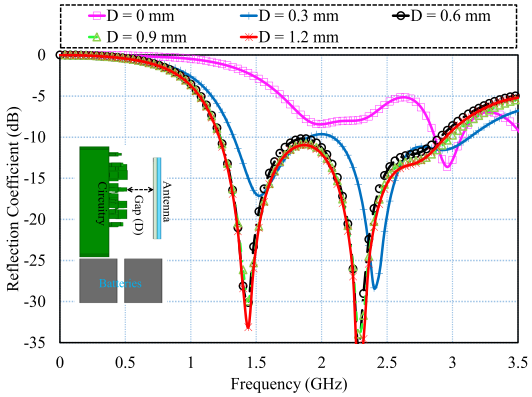

FIGURE 15. Coupling effects due to metallic components of the system on the ultra-wideband antenna performance.

IV. LINK BUDGET CALCULATION

The determination of the telemetry range between the implantable device and exterior base station is vital to transfer the biological information reliably. However, various types of losses are associated with the link budget calculations, namely free space losses, cable losses, and antenna material and mismatch losses [34]. We determined the link margins from the difference between the antenna power (A_P) and the required antenna power (R_P) based on the Friis equation, and the link margin should be greater than 20 dB for consistent communication. The key parameters used in these calculations are given in Table 6. R_P can be computed as follows.

$$R_P = \frac{E_b}{N_o} + KT + B_r \tag{5}$$

TABLE 6. Link budget parameters of the proposed antenna.

Symbol	Quantity	Value
P_a	Transmitter power (dBm)	-16
N_o	Noise power density:(dB/Hz)	-20.93
T	Temperature (Kelvin)	273
f	Resonating frequency	2.45 GHz
G_a	Transmitter antenna gain (dBi)	Tissue dependent
G_b	Receiver antenna gain (dBi)	2
L	Free space loss (dB)	Distance dependent
A_P	Available power (dB)	Distance dependent
R_P	Required power (dB)	-155.9
A_p -R_p	Margin (dB)	Fig. 16

where E_b/N_o, K, T_o, and B_r represent the phase shift keying, Boltzmann's constant, temperature, and bit rate, respectively. On the other hand, A_p can be calculated as

$$A_P(dB) = P_a + G_a + G_b + L_f \tag{6}$$

where P_a, G_a, and G_b represent the transmitted power, implantable antenna gain, and receiver monopole antenna gain, respectively. L_f represents the free space losses and can be computed from the following formula.

$$L(dB) = 20log(\frac{4\pi d}{\lambda}) \tag{7}$$

where d is the distance between the implantable antenna and the outside controlling device, which can vary from 2 to 5 meters. It is noteworthy that the European research council restricts the input power to 25 μW and the $EIRP_{max}$ for the ISM (2.45 GHz) band to 20 dBm [15] for the safety of patients. The in-body communication range was computed for the ISM (2.45 GHz) band. The primary concerns of the IMDs are battery power availability and circuitry. Depending on the application of the proposed antenna based on the input power, the skin implantation is taken into consideration. Based on the skin implantable devices, the assumed transmitted power P_t is -16 dBm and the bit rate B_r of the proposed antenna is 1 Mbps. The distance versus margin graph for the proposed implantation scenarios is shown in Fig. 16. It can be shown from Fig. 16, that with the input power (-16 dBm), 1 Mbps of data could be transmitted over more than 15 m distance. It is observed that the range of data transmission could be changed by increasing or decreasing the data rate and gain.

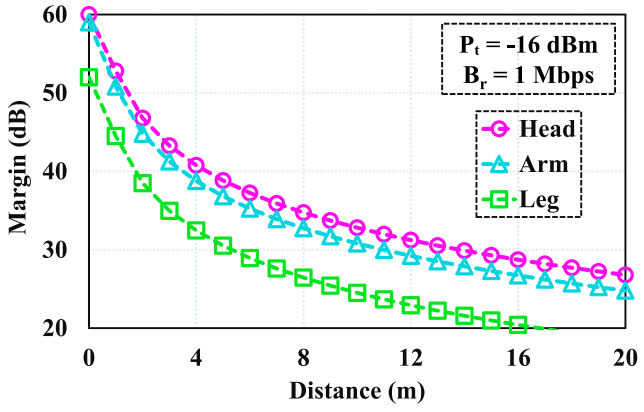

FIGURE 16. Link budget for different implant locations in ISM (2.45 GHz) band.

V. CONCLUSION

An ultra-miniaturized and ultra-wideband implantable antenna based device operating at 2.45 GHz was designed in this study. The proposed antenna was primarily developed for overcoming the detuning phenomenon that may occur owing to human tissue heterogeneity, tissue property variations with age, and circuitry of the IMDs. The open-ended slots in the patch and ground of the antenna, were noticed to be crucial for frequency tuning, impedance matching, and miniaturization. The results obtained in the HSP were verified by implanting the antenna and its corresponding system in different organs of a heterogeneous human model. The investigation of the SAR assured the patient safety by achieving compliance with the IEEE C95.1-1999 guidelines in the implanted locations. To determine the telemetry range between the ultra-wideband antenna system and the outside base station, the link margins were calculated for the prescribed implant locations. The simulated and measured results confirmed that the suggested ultra-wideband antenna system is suitable, and indeed, beneficial for practical implementation.

REFERENCES

[1] T. Karacolak, A. Z. Hood, and E. Topsakal, "Design of a dual-band implantable antenna and development of skin mimicking gels for continuous glucose monitoring," *IEEE Trans. Microw. Theory Techn.*, vol. 56, no. 4, pp. 1001–1008, Apr. 2008.

[2] K. Gosalia, G. Lazzi, and M. Humayun, "Investigation of a microwave data telemetry link for a retinal prosthesis," *IEEE Trans. Microw. Theory Techn.*, vol. 52, no. 8, pp. 1925–1933, Aug. 2004.

[3] S. H. Lee, J. Lee, Y. J. Yoon, S. Park, C. Cheon, K. Kim, and S. Nam, "A wideband spiral antenna for ingestible capsule endoscope systems: Experimental results in a human phantom and a pig," *IEEE Trans. Biomed. Eng.*, vol. 58, no. 6, pp. 1734–1741, Jun. 2011.

[4] F. Faisal, M. Zada, A. Ejaz, Y. Amin, S. Ullah, and H. Yoo, "A miniaturized dual-band implantable antenna system for medical applications," *IEEE Trans. Antennas Propag.*, vol. 68, no. 2, pp. 1161–1165, Feb. 2020.

[5] H. Bahrami, S. A. Mirbozorgi, R. Ameli, L. A. Rusch, and B. Gosselin, "Flexible, polarization-diverse UWB antennas for implantable neural recording systems," *IEEE Trans. Biomed. Circuits Syst.*, vol. 10, no. 1, pp. 38–48, Feb. 2016.

[6] F. Kong, M. Zada, H. Yoo, and M. Ghovanloo, "Adaptive matching transmitter with dual-band antenna for intraoral tongue drive system," *IEEE Trans. Biomed. Circuits Syst.*, vol. 12, no. 6, pp. 1279–1288, Dec. 2018.

[7] L.-J. Xu, Y.-X. Guo, and W. Wu, "Bandwidth enhancement of an implantable antenna," *IEEE Antennas Wireless Propag. Lett.*, vol. 14, pp. 1510–1513, 2015.

[8] R. Das, F. Moradi, and H. Heidari, "Biointegrated and wirelessly powered implantable brain devices: A review," *IEEE Trans. Biomed. Circuits Syst.*, vol. 14, no. 2, pp. 343–358, Apr. 2020.

[9] B. Chi, J. Yao, S. Han, X. Xie, G. Li, and Z. Wang, "A 2.4 GHz low power wireless transceiver analog front-end for endoscopy capsule system," *Anal. Integr. Circuits Signal Process.*, vol. 51, no. 2, pp. 59–71, May 2007.

[10] B. Chi, J. Yao, S. Han, X. Xie, G. Li, and Z. Wang, "Low-power transceiver analog front-end circuits for bidirectional high data rate wireless telemetry in medical endoscopy applications," *IEEE Trans. Biomed. Eng.*, vol. 54, no. 7, pp. 1291–1299, Jul. 2007.

[11] *Technical and Operating Parameters and Spectrum Use for Short-Range Radiocommunication Devices*. Accessed: Sep. 22, 2020. [Online]. Available: https://www.itu.int/pub/R-REP-SM.2153-7-2019

[12] S. Hashemi and J. Rashed-Mohassel, "Miniaturization of dual band implantable antennas," *Microw. Opt. Technol. Lett.*, vol. 59, no. 1, pp. 36–40, Jan. 2017.
[13] H. Zhang, L. Li, C. Liu, Y.-X. Guo, and S. Wu, "Miniaturized implantable antenna integrated with split resonate rings for wireless power transfer and data telemetry," *Microw. Opt. Technol. Lett.*, vol. 59, no. 3, pp. 710–714, Mar. 2017.
[14] C. Liu, Y.-X. Guo, and S. Xiao, "A hybrid patch/slot implantable antenna for biotelemetry devices," *IEEE Antennas Wireless Propag. Lett.*, vol. 11, pp. 1646–1649, 2012.
[15] F. Faisal and H. Yoo, "A miniaturized novel-shape dual-band antenna for implantable applications," *IEEE Trans. Antennas Propag.*, vol. 67, no. 2, pp. 774–783, Feb. 2019.
[16] A. Basir, M. Zada, and H. Yoo, "Compact and flexible wideband antenna for intraoral tongue-drive system for people with disabilities," *IEEE Trans. Antennas Propag.*, vol. 68, no. 3, pp. 2405–2409, Mar. 2020, doi: 10.1109/TAP.2019.2943416.
[17] C.-M. Lee, T.-C. Yo, F.-J. Huang, and C.-H. Luo, "Bandwidth enhancement of planar inverted-F antenna for implantable biotelemetry," *Microw. Opt. Technol. Lett.*, vol. 51, no. 3, pp. 749–752, Mar. 2009.
[18] C.-L. Tsai, K.-W. Chen, and C.-L. Yang, "Implantable wideband low-SAR antenna with C-Shaped coupled ground," *IEEE Antennas Wireless Propag. Lett.*, vol. 14, pp. 1594–1597, 2015.
[19] S. Das and D. Mitra, "A compact wideband flexible implantable slot antenna design with enhanced gain," *IEEE Trans. Antennas Propag.*, vol. 66, no. 8, pp. 4309–4314, Aug. 2018.
[20] R. Das and H. Yoo, "A wideband circularly polarized conformal endoscopic antenna system for high-speed data transfer," *IEEE Trans. Antennas Propag.*, vol. 65, no. 6, pp. 2816–2826, Jun. 2017.
[21] Y. Fan, J. Huang, T. Chang, and X. Liu, "A miniaturized four-element MIMO antenna with EBG for implantable medical devices," *IEEE J. Electromagn., RF Microw. Med. Biol.*, vol. 2, no. 4, pp. 226–233, Dec. 2018.
[22] S. Hout and J.-Y. Chung, "Design and characterization of a miniaturized implantable antenna in a seven-layer brain phantom," *IEEE Access*, vol. 7, pp. 162062–162069, Nov. 2019.
[23] C. Liu, Y.-X. Guo, R. Jegadeesan, and S. Xiao, "*In vivo* testing of circularly polarized implantable antennas in rats," *IEEE Antennas Wireless Propag. Lett.*, vol. 14, pp. 783–786, 2015.
[24] W. Cui, R. Liu, L. Wang, M. Wang, H. Zheng, and E. Li, "Design of wideband implantable antenna for wireless capsule endoscope system," *IEEE Antennas Wireless Propag. Lett.*, vol. 18, no. 12, pp. 2706–2710, Dec. 2019.
[25] S.-M. Huang, M.-R. Tofighi, and A. Rosen, "Considerations for the design and placement of implantable annular slot antennas for intracranial pressure monitoring devices," *IEEE Antennas Wireless Propag. Lett.*, vol. 14, pp. 1514–1517, Nov. 2015.
[26] K. N. Ketavath, D. Gopi, and S. Sandhya Rani, "*In-vitro* test of miniaturized CPW-fed implantable conformal patch antenna at ISM band for biomedical applications," *IEEE Access*, vol. 7, pp. 43547–43554, 2019.
[27] X.-T. Yang, H. Wong, and J. Xiang, "Polarization reconfigurable planar inverted-F antenna for implantable telemetry applications," *IEEE Access*, vol. 7, pp. 141900–141909, 2019.
[28] G. Z. Yang, Ed., *Body Sensor Networks*. London, U.K.: Springer-Verlag, 2006.
[29] H.-Y. Lin, M. Takahashi, K. Saito, and K. Ito, "Performance of implantable folded dipole antenna for in-body wireless communication," *IEEE Trans. Antennas Propag.*, vol. 61, no. 3, pp. 1363–1370, Mar. 2013.
[30] S. Ullah, H. M. A. Higgin Siddiqui, and K. Kwak, "A study of implanted and wearable body sensor networks," in *Agent and Multi-Agent Systems: Technologies and Applications* (Lecture Notes in Computer Science), vol. 4953. Berlin, Germany: Springer, 2008, pp. 464–473.
[31] Z.-J. Yang, L. Zhu, and S. Xiao, "An implantable wideband microstrip patch antenna based on high-loss property of human tissue," *IEEE Access*, vol. 8, pp. 93048–93057, May 2020.
[32] M. Zada, I. A. Shah, A. Basir, and H. Yoo, "Ultra-compact implantable antenna with enhanced performance for leadless cardiac pacemaker system," *IEEE Trans. Antennas Propag.*, vol. 69, no. 2, pp. 1152–1157, Feb. 2021, doi: 10.1109/TAP.2020.3008070.
[33] M. Zada and H. Yoo, "A miniaturized triple-band implantable antenna system for bio-telemetry applications," *IEEE Trans. Antennas Propag.*, vol. 66, no. 12, pp. 7378–7382, Dec. 2018.
[34] S. A. A. Shah and H. Yoo, "Scalp-implantable antenna systems for intracranial pressure monitoring," *IEEE Trans. Antennas Propag.*, vol. 66, no. 4, pp. 2170–2173, Apr. 2018.
[35] S. Hayat, S. A. A. Shah, and H. Yoo, "Miniaturized dual-band circularly polarized implantable antenna for capsule endoscopic system," *IEEE Trans. Antennas Propag.*, early access, Oct. 8, 2020, doi: 10.1109/TAP.2020.3026881.
[36] M. Zada, I. A. Shah, and H. Yoo, "Metamaterial-loaded compact high-gain dual-band circularly polarized implantable antenna system for multiple biomedical applications," *IEEE Trans. Antennas Propag.*, vol. 68, no. 2, pp. 1140–1144, Feb. 2020.
[37] I. A. Shah, M. Zada, and H. Yoo, "Design and analysis of a compact-sized multiband spiral-shaped implantable antenna for scalp implantable and leadless pacemaker systems," *IEEE Trans. Antennas Propag.*, vol. 67, no. 6, pp. 4230–4234, Jun. 2019.

MUHAMMAD YOUSAF received the B.Sc. degree in electronics engineering from the University of Engineering and Technology (UET) Taxila, Pakistan, in 2014, and the M.Sc. degree in electrical engineering from COMSATS University Islamabad, Wah Campus, in 2017. He is currently pursuing the Ph.D. degree with UET Taxila. He is also working under the ACTSENA Research Group focused on implantable antennas and systems, RF coils, wireless power transfer, image processing, and passive chipless RFID tags.

ISMAIL BEN MABROUK (Senior Member, IEEE) received the B.A.Sc. and M.A.Sc. degrees in electrical engineering from the University of Lille, Lille, France, in 2006 and 2007, respectively, and the Ph.D. degree in electrical engineering from the University of Quebec, Canada, in 2012. From 2007 to 2009, he was with Huawei Technologies, Paris, France. In 2012, he joined the Wireless Devices and Systems (WiDeS) Group, University of Southern California, Los Angeles, USA. He is currently an Assistant Professor with Durham University, Durham, U.K. His research interests include implantable and wearable antenna design, propagation studies for multiple-input and multiple-output (MIMO) systems at the millimiter-wave and THz frequencies, deep learning, and wireless body area network for medical applications. He was a recipient of the Abu Dhabi Award for Research Excellence (AARE).

MUHAMMAD ZADA received the B.Sc. degree in telecommunication engineering from the University of Engineering and Technology Peshawar, Peshawar, Pakistan, in 2015. He is currently pursuing the M.S./Ph.D. degrees in electronic engineering with Hanyang University, Seoul, South Korea.

He has published more than 15 articles in high-quality journals and conference proceedings in the field of telecommunications, biomedical, and electronic engineering. His current research interests include implantable antennas and devices, intra-oral tongue drive system, wireless power transfer, millimeter-wave antennas, MIMO antenna systems, wearable sensors and antennas, MRI and RF coils, microwave breast cancer detection, frequency-selective surfaces, and EBGs. He received the Best Student Paper Competition 2018 by the Korean Institute of Electromagnetic Engineering & Science (KIEES). He is serving as a reviewer for IEEE Transactions, RFCAD, and Elsevier journals.

ADEEL AKRAM received the B.S. degree in electrical engineering from the University of Engineering and Technology Lahore, Pakistan, in 1995, the M.S. degree in computer engineering from the National University of Sciences and Technology (NUST), Pakistan, and the Ph.D. degree in electrical engineering from the University of Engineering and Technology Taxila, Pakistan, in 2000 and 2007, respectively. He is currently the Dean and a Professor of the Telecommunication Engineering Department, University of Engineering and Technology Taxila. His research interests include microwave and communication systems and is leading a 5G wireless communication group at UET Taxila.

YASAR AMIN (Senior Member, IEEE) received the B.Sc. degree in electrical engineering (with specialization in telecommunication) and the M.B.A. degree in innovation and growth from the Turku School of Economics, University of Turku, Finland, and the M.Sc. degree in electrical engineering (with specialization in system on chip design) and the Ph.D. degree in electronic and computer systems from the Royal Institute of Technology (KTH), Sweden, with the research focus on printable green RFID antennas for embedded sensors. He is currently a Professor and the Chairman of the Telecommunication Engineering Department, University of Engineering and Technology Taxila, Pakistan. He also serves as the Director for the Embedded Systems Research and Development Centre. He is also the Founder of the Agile Creative Technologies for Smart Electromagnetic Novel Applications (ACTSENA) research group. He has authored or coauthored more than 100 international technical articles in conferences and journals. His research interests include the design and application of multiple antenna systems for next generation mobile communication systems, millimeter-wave and terahertz antenna array, implantable & wearable electronics, and inkjet printing technology in microwave applications. He is a member of more than a dozen international professional societies and the Fellow of PAE.

MOURAD NEDIL (Senior Member, IEEE) received the Dipl. Ing. degree from the University of Algiers (USTHB), Algiers, Algeria, in 1996, the D.E.A. (M.S.) degree from the University of Marne la Vallée, Marne la Vallée, France, in 2000, and the Ph.D. degree from the Institut National de la Recherche Scientifique (INRS-EMT), Université de Québec, Montreal, QC, Canada, in April 2006. He received a Postdoctoral Fellowship from the INRS-EMT, RF Communications Systems Group, from 2006 to 2008.

In June 2008, he joined the Engineering School department, University of Quebec at Abitibi-Témiscamingue, Quebec, Canada, where he is currently a Full Professor. His research interests include antennas, MIMO radio-wave propagation, and microwave devices.

HYOUNGSUK YOO (Senior Member, IEEE) received the B.Sc. degree in electrical engineering from Kyungpook National University, Daegu, South Korea, in 2003, and the M.Sc. and Ph.D. degrees in electrical engineering from the University of Minnesota, Minneapolis, MN, USA, in 2006 and 2009, respectively.

In 2009, he joined the Center for Magnetic Resonance Research, University of Minnesota, as a Postdoctoral Associate. In 2010, he joined Cardiac Rhythm Disease Management, Medtronic, MN, USA, as a Senior EM/MRI Scientist. From 2011 to 2018, he was an Associate Professor with the Department of Biomedical Engineering, School of Electrical Engineering, University of Ulsan, Ulsan, South Korea. Since 2018, he has been an Associate Professor with the Department of Biomedical Engineering and the Department of Electronic Engineering, Hanyang University, Seoul, South Korea. He has been the CEO of E2MR, Seoul, a startup company, since 2017. His current research interests include electromagnetic theory, numerical methods in electromagnetics, metamaterials, antennas, implantable devices, and magnetic resonance imaging in high-magnetic field systems.

Dr. Yoo was a recipient of the Third Prize for the Best Student Paper at the 2010 IEEE Microwave Theory and Techniques Society International Microwave Symposium.